ACTA METALLURGICA SLOVACA
2025, VOL. 31, NO. 1, 42-46

RESEARCH PAPER

Pressings shape evaluation by modern contactless methods

Miroslav Tomáš[1], Marek Buber[1], Juliy Martyn Kulya[1], Juraj Sulaček[2], Emil Evin[1], Michal Fabian[1]*

[1] Technical University of Košice, Faculty of Mechanical Engineering, Department of Automotive Production, Mäsiarska 74, 040 01 Košice, Slovakia

[2] 3Dees Industries Slovakia s.r.o., Haburská 49D, 821 01 Bratislava-Ružinov, Slovakia

*Corresponding author: miroslav.tomas@tuke.sk, Tel.:+421 55 602 3524, Faculty of Mechanical Engineering, Technical University of Košice, Mäsiarska 74, 040 01 Košice, Slovakia

Received: 28.11.2024
Accepted: 04.02.2025

ABSTRACT

As part of the Industry 4.0 concept, companies are adopting new processes that utilize contactless methods to assess the shapes of pressings. Evaluating the pressings is essential due to the springback phenomena that occur after plastic deformation, which is more pronounced when high-strength steels are used in car bodies. Although photogrammetric methods based on 2D images have been used in the industry for over a decade, 3D optical scanning methods are preferred because they offer increased precision. This article evaluated cylindrical pressings made of dual-phase steel DP800 with a thickness of 1.6 mm—specifically flat-bottomed and hemispherical-bottomed cups. The shape of the pressings was determined using optical scanning with the GOM Scan 1 device alongside a photogrammetric system called ARGUS. The surfaces obtained from both methods were then compared to assess the accuracy of the scanned surface against the real surface acquired through photogrammetry. The scanned surfaces of the pressings were also used to compare the results of numerical simulations conducted in PamStamp software. In these simulations, the material was modelled using two sets of constitutive laws: the Hill48 yield law combined with the Hollomon hardening law as the first set and the Vegter Lite yield law combined with the Krupkowski hardening law as the second set. Real cups with a diameter of 50 mm were created using a deep-drawing process on the Erichsen 145-60 testing machine, starting with a blank diameter of 90 mm and lubricated with plastic foil to preserve the electrochemically etched grid. A comparison between the scanned surfaces and the real surfaces obtained through photogrammetry showed a strong correlation, validating 3D scanning as an effective method for evaluating pressing shapes. Furthermore, comparing the scanned surfaces with the results of the numerical simulations demonstrated similar findings for both sets of constitutive laws used to model the dual-phase steel in the experiments.

Keywords: flat and hemispherical bottomed cup, photogrammetry, 3D scanning, numerical simulation, shape comparison

INTRODUCTION

In the automotive industry, many parts of the car body are made of sheet metal forming. Stamping, i.e., deep drawing, is the main process determining the final shape of the pressings. Thus, the formability of material and process parameters, such as die geometry, friction, blank holder force, browbeat force position, etc. [1,2], are the main factors in deep drawing.

The Industry 4.0 concept uses various measurement tools and methods for product quality assurance based on a reliable digital representations of products, processes and production systems. Photogrammetry and 3D optical scanning digitizes physical models into CAD formats using specialized devices and software [3]. Intelligent automated contactless inspection equipment minimizes inspection time compared to the standard contact coordinate measurements while ensuring continuous process quality monitoring [4,5]. Photogrammetric systems are designed to process 2D digital images into spatial data by triangulation, thus reconstructing the surface of an object into a 3D object, that closely resembles the original in its dimensions [6,7]. The method of scanning object surfaces has also been found to measure the deformation characteristics of materials [8] and to monitor dynamics of structures [9].

Vagovský et al. [10] evaluated the measuring ability of the GOM ATOS Triple Scan II 3D scanner using different measuring volumes. They found a very small measurement deviation, and the ATOS Triple scan II scanner could not achieve the result. However, they also stated that they brought applications to other areas of use, such as medium-sized and large-sized parts, which can provide excellent measurement results. Mendricky [11] focused on a complete analysis of the accuracy of digitizing objects using different scanners. He performed the study on ATOS II MV400 and RevScan laser scanners, where he analyzed the capabilities of the scanners in non-laboratory conditions on samples of complex shapes. He found that the scanners above can be used in non-laboratory conditions to check industrial products' dimensional and shape accuracies [11].

The pressings shape is also important from the view of adjacent parts in the car body structure. All input parts entering the process must be shaped and dimensionally accurate when welding a body. Otherwise, internal stress could occur in a car's body, affecting its integrity [12]. Therefore, it is very important to consider the springback when pressing body parts [13,14]. The size of the springback has a fundamental impact on the precision of the final product [15]. Firat et al. investigated the improvement of deformation accuracy based on FE analysis of the engine mounting bracket pressing process, including springback deformations. Lee et al. [16] studied the developed tensile force and elastic properties of the omega (Ω) profile material used in the experiment. Their proposed plasticity model outperformed the isotropic hardening and thickness change distribution models in predicting the springback. Carden et al. [17] compared the curvature angles of the radius formed on experimental specimens of DQSK steel, HSLA steel, and 6022-T4 aluminium alloys. When comparing the radius after springback, they found that DQSK steel has the lowest springback, but the difference was almost negligible compared to HSLA steel. Frącz and Stachowicz [18], in their study, experimentally presented broader aspects of the use of the GOM Argus photogrammetric system. In their research, they state that the Argus system can be used for initial FLC curves, evaluation of the forming process, determination of the actual deformation, estimation of thinning during sheet metal drawing, etc. to provide accuracy of determination even when using a denser measuring dot-net. Heng et al. [19] investigated the accuracy of constitutive mathematical models and simulations based on the implications of these models. They found that the simulation with the implied Hill´48- r constitutive model showed the smallest deviation compared to the experiment. This deviation can be further reduced using the NARF Hill´48 model. On the contrary, Oberkampf et al [20] investigated the accuracy of mathematical models of simulations that deal with the numerical solution of a set of partial differential equations (PDEs). Mulidran et al. [21] studied the effect of a combination of various yield laws and hardening laws on the springback prediction at bending by the numerical simulation. They found a better correlation between the Ludwik hardening law and the yield law used in the study.

The paper compares the real surface of dual-phase steel pressings reached by the photogrammetric system Argus and optical scanning. Then, the surface reached by optical scanning will be used to evaluate numerical simulation results for different constitutive models of dual-phase steel.

MATERIAL AND METHODS

Material properties

In the article, cylindrical pressings made of dual-phase steel DP800 with thickness 1.6 mm - flat bottomed and hemisperical bottomed cups were evaluated. The pressing shape was determined by optical scanning using GOM Scan 1 and photogrammetric system ARGUS. These were compared to the results of numerical simulation in PamStamp software when the Vegter Lite yield law and Krupkowski hardening law modeled material. Real cups (pressings) of 50 mm diameter were deeply drawn on the Erichen 145-60 testing machine from a blank diameter of 90 mm and lubricated with plastic foil to preserve the electrochemically etched grid. The results allowed for determining the pressing accuracy, cup shape, and deviation of the real pressing shape and numerical simulation.

Dual-phase steel DP800 was tested in experiments with a thickness of 1.6 mm. The steel's chemical composition is shown in **Table 1**. Mechanical properties, shown in **Table 2**, were measured by standards ISO 6892-1 [22], plastic strain ratios according to standard ISO 10113 [23], and strain-hardening exponent and strength constant according to standard ISO 10250 [24] within the range yield strength elongation-uniform elongation.

Table 1 Chemical composition of dual phase steel DP800 [wt.%]

C_{max}	Si_{max}	Mn_{max}	P_{max}	S_{max}	Al_{total}	Cr+Mo max	Nb+Ti max
0.170	0.3	2.000	0.050	0.010	0.015-0.08	1.000	0.050

Table 2 Mechanical properties of dual phase steel DP800 (rolling dir.)

Property	$R_{p0.2}$ [MPa]	Rm [MPa]	Ag [%]	A_{80} [%]	n [-]	K [MPa]	r_0 [-]	r_{45} [-]	r_{90} [-]
Value	527	828	12.5	19.9	0.125	1219	0.873	0.907	0.979
Std. Dev.	3	2	0.5	0.5	0.001	3.4	0.028	0.022	0.030

Cups of 50 mm in diameter were deep drawn on Erichsen 145-60 testing machine. Two cups – flat bottomed and hemispherical (**Fig. 1** and **Fig. 2**) – were deep drawn with blankholder force of 25 kN applied and lubricated by plastic foil to preserve etched dots. Drawing die diameter D_d was 54.8 mm, die radius r_d 3 mm, punch diameter d_p 50 mm, punch radius for flat bottomed cup r_p = 7 mm; punch radius for hemispherical bottomed cup r_p = 25 mm. Blank diameter D_0 was 90 mm; thus, the drawing ratio D0/dp = 1.8 for both cup shapes.

Fig. 1 Flat bottomed cups

Fig. 2 Hemispherical bottomed cups

Photogrammetric system ARGUS

Specimens for deep drawing were prepared by cutting square blanks 110x100 mm. Then, a deformation grid of dots of 1 mm size and spacing of 2 mm was applied by electrochemical etching using the Oestling EU Classic 300 device and electrolyte 639 for Zn-coated metal sheets. After deep drawing, the Argus photogrammetric system was used to evaluate the shape of the cups (**Fig. 3**). After data processing in the Argus 6.3 software, the shape of the cup as a mesh surface was exported in STL file format.

Fig. 3 Photogrammetric system Argus

Optical scanner GOM Scan 1

The second method to evaluate the shape of the cups was contactless scanning—the GOM Scan 1 device (**Fig. 4**) scanned cups after deep drawing with volume MV 400. Then, using the software Zeiss Inspect Pro (**Fig. 5**), 3D models were created. The device allows for scanning 6 million points in an area of 400x250 mm with an accuracy of 0.02 mm, as measured [25]. Before scanning, cups were placed on a rotary table at the correct distance from the scanner. To ensure proper overlap of the scans, reference points were stuck to the sample, which guaranteed accurate positioning of the scanned layers. The rotary table rotated by 45° and 8 scans were done for each side (outside, inside). Based on the reference points, 3D model of cups was polygonised by the software and exported in STL file format.

Fig. 4 Photogrammetric system GOM Scan 1 MV400

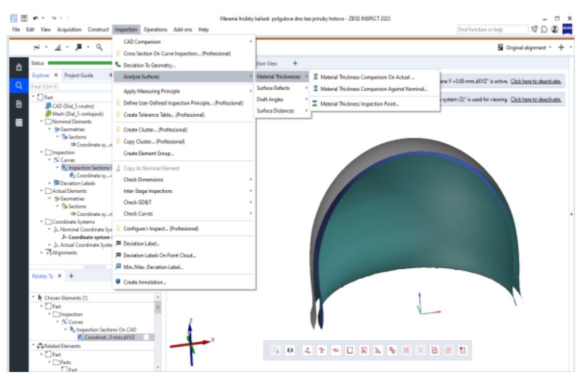

Fig. 5 Data processing in ZEISS INSPECT Pro software

Numerical simulation

A simulation model of the deep drawing process was created in a PamStamp simulation software by ESI. 3D die, punch, and blank holder models created according to real dimensions were imported and meshed into the software. The blankholder force was set to 25 kN and friction coefficient 0.05 corresponded to deep drawing with plastic foil with 0.05 mm thickness [26]. Material (i.e. blank properties) was described by two constitution equations as follows:

1. Hill48 yield law [27]

$$\sigma_1^2 - \frac{2.r_0}{1+r_0}\sigma_1.\sigma_2 + \frac{r_0(1+r_{90})}{r_{90}(1+r_0)}\sigma_2^2 = \sigma_{1y}^2 \quad (1.)$$

and Hollomon hardening law [28]

$$\sigma_{true} = K.\varphi^n \quad (2.)$$

where σ_1, σ_2 [MPa] are major and minor true stress; r_0, r_{45} and r_{90} [-] are plastic strain ration in 0°, 45 and 90° to rolling direction; σ_{1y}^2 [MPa] is the uniaxial yield stress; σ_{true} [MPa] is true stress; φ [-] is true strain; K [MPa] is strength constant and n [-] is strain-hardening exponent.

2. Vegter Lite [29]

$$\begin{pmatrix}\sigma_1\\ \sigma_2\end{pmatrix} = \frac{(1+\lambda^2)\begin{pmatrix}\sigma_1\\ \sigma_2\end{pmatrix}_i^r + w.2.\lambda.(1-\lambda).\begin{pmatrix}\sigma_1\\ \sigma_2\end{pmatrix}_i^h + \lambda^2.\begin{pmatrix}\sigma_1\\ \sigma_2\end{pmatrix}_{i+1}^r}{(1-\lambda)^2 + w.2.\lambda.(1-\lambda) + \lambda^2} \quad (3.)$$

and Kupkowski hardening law [30,31]

$$\sigma_{true} = K.(\varphi_0 + \varphi^n) \quad (4.)$$

where σ_1, σ_2 [MPa] are major and minor true stress; λ [-] is Bezier interpolation factor; w [-] is weight factor depending on material (steel or aluminum) and defining shear weight and plane strain weight; σ_{true} [MPa] is true stress; φ [-] is true strain; φ_0 [-] is offset strain; K [MPa] is strength constant and n [-] is strain-hardening exponent. It should be noted that K and n are not the same for both hardening models. Yield loci are compared in **Fig. 6**.
Parameters of models were calculated using a MatWizard function based on measured material properties as specified in **Table 2**. In the simulation, springback was calculated after a deep drawing process. Then, the surface was exported as a mesh surface in STL file format.

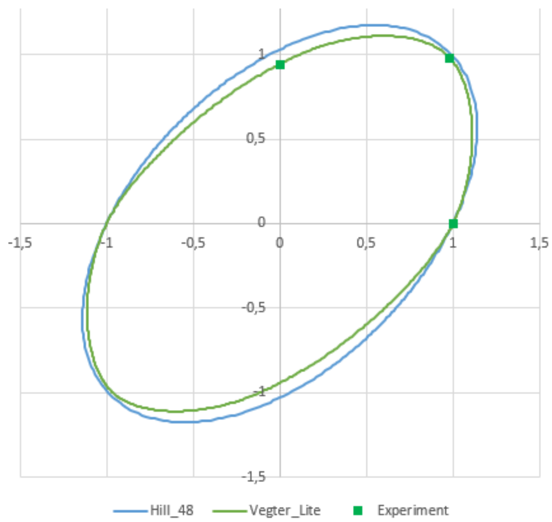

Fig. 6 Comparison of yield locus

Zeiss Inspect Pro software compared surfaces resulting from numerical simulation, measurement by system Argus, and optical scanning. The scanned surface was set as a reference because it is a real surface of the part. **Table 4** shows the results of maximum and minimum deviation from the scanned surface and calculated tolerance.

RESULTS AND DISCUSSION

To verify the scanning precision, surfaces resulting from Argus software were first compared to the scanned surface of the pressings. Results can be seen in **Fig. 7** and **Fig. 8**, respectively. Deviation of surfaces was evaluated at 0°, 45, and 90° to the rolling direction. The flat-bottomed cup has shown a deviation in the rolling direction (0°) +0.04 to -0.07 mm; in the 45° direction, it was +0.03 to -0.07 mm, and in 90° directions, it was +0.01 to -0.07 mm. The hemispherical bottomed cup has shown deviations in the rolling direction within -0.06 to 0 mm; in 45°, it was +0.03 to -0.06 mm, and in the 90° direction, it was +0.03 to -0.06 mm. Thus, the precision of the scanning surface should be considered within a 0.1 mm tolerance window. It is affected mainly by the measuring volume applied at 3D scanning [10,11].
In both cases, surfaces show visible deviations in the position of dots etched before deformation. Due to friction during deep drawing, the Argus photogrammetric system did not recognise some dots, and thus, a complete surface was not reached. Also, the surface Argus reaches is not complete toward the edge of the cup in both cases.
A good correlation between Argus surfaces and scanned surfaces might be reached. Then, scanned surfaces can be applied as a nominal surface when evaluating the numerical simulation results. Compared to the surface reached by the Argus system, it is more complete than the surface evaluated by the Argus system. However, it might have also resulted from light conditions when taking the pictures for evaluation in the Argus system.

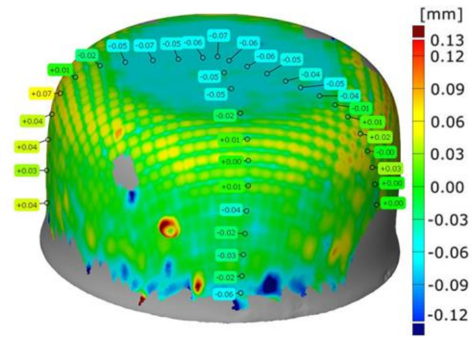

Fig. 7 Inspection results for the flat-bottomed cup: scan-Argus

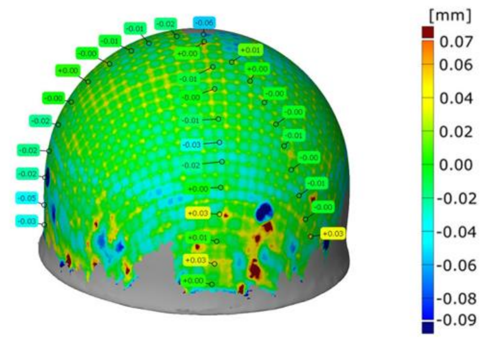

Fig. 8 Inspection results for the hemispherical-bottomed cup: scan-Argus

Inspection results, as the scanned surface to the simulation surface comparison for the flat-bottomed cup, are presented in **Fig. 9** and **Fig. 10**, respectively. The directional dependence of evaluated maximal and minimal deviation is shown in **Table 3**. When considering Hill48/Hollomon constitutive equations, the gap between max. and min. varies as follows: 0.35 mm, 0.29 mm, and 0.34 mm. For Vegter Lite/Krupkowski constitutive equations, the gap between max. and min. deviation varies: 0.37 mm, 0.39 mm, and 0.50 mm. Thus, the lower deviations have been found for Hill48/Hollomon constitutive equations for flat-bottomed cup.

Table 3 Comparison of scanned surface to simulation results for the flat-bottomed cup

	Hill48/Hollomon			Vegter Lite/Krupkowski		
Roll.dir.	0°	45°	90°	0°	45°	90°
Max. dev.	+0.06	+0.14	+0.04	+0.03	+0.19	+0.11
Min. dev.	-0.29	-0.15	-0.30	-0.34	-0.20	-0.39
Max-Min	0.35	0.29	0.34	0.37	0.39	0.50

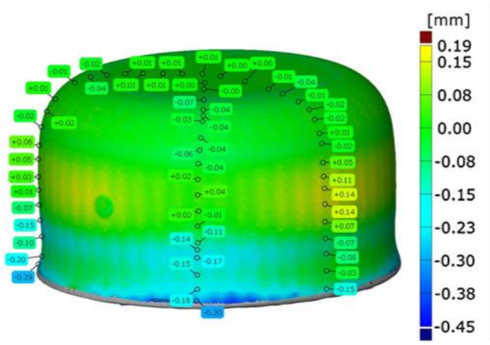

Fig. 9 Inspection results for the flat-bottomed cup: scan to Hill48/Hollomon

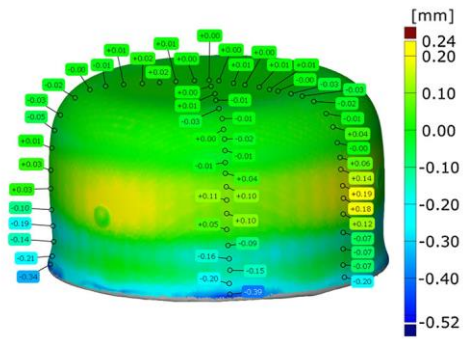

Fig. 10 Inspection results for the flat-bottomed cup: scan to Vegter/Krupkowski

Inspection results for the hemispherical bottomed cup are presented in **Fig. 11** and **Fig. 12**, respectively. The directional dependence of evaluated maximal and minimal deviation is shown in **Table 4**. Thus, Hill48/Hollomon constitutive equations showed the gap between max. and min. deviation as follows: 0.29 mm, 0.25 mm, and 0.41 mm. Vegter Lite/Krupkowski constitutive equations showed the gap between max. and min. deviation as follows: 0.37 mm, 0.30 mm, and 0.28 mm. So, similarly to the flat-bottomed cup, lower deviations have also been found for Hill48/Hollomon constitutive equations.

Table 4 Comparison of scanned surface to simulation results for the hemispherical-bottomed cup

	Hill48/Hollomon			Vegter Lite/Krupkowski		
Roll.dir.	0°	45°	90°	0°	45°	90°
Max. dev.	+0.03	+0.02	+0.05	+0.03	+0.11	+0.03
Min. dev.	-0.26	-0.23	-0.36	-0.34	-0.19	-0.25
Max-Min	0.29	0.25	0.41	0.37	0.30	0.28

The selection of constitutive equations for modelling material behaviour in deep-drawing numerical simulations is very important. While for standard low carbon steels, using the Hill 48 and Hollomon hardening equations is good enough to describe their anisotropy and hardening, mainly due to the ease of their construction from mechanical properties, Vegter proposed new criteria that can explain the yielding and hardening behavior of other materials, such as AHSS steels, stainless steel, and aluminum alloys as well [32]. The difference in yield loci, as shown in **Fig. 6**, has influenced the results from the view of the final shape of the pressings. Otherwise, the hardening rule and the strain-hardening model influence the results [33].

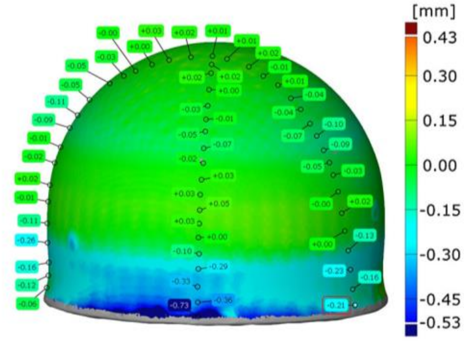

Fig. 11 Inspection results for the hemispherical-bottomed cup: scan to Hill48/Hollomon

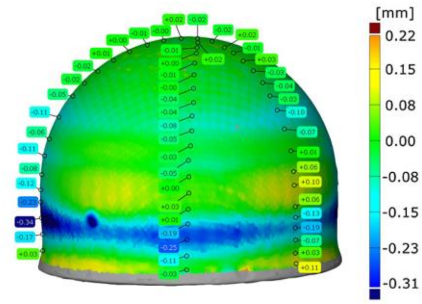

Fig. 12 Inspection results for the hemispherical-bottomed cup: scan to Vegter/Krupkowski

The results came from the isotropic hardening rule, which implies that the yield surface expands without changing shape as the plastic strain increases [33]. A difference in results should also be caused by the strain hardening models applied because of the small difference in true stress calculated by Eq. (2.) and Eq. (4.) up to the strain level of 0.06, as shown in **Fig. 13** [34]. More precise results should be expected when kinematic or isotropic-kinematic rules are applied, as Mulidran proved at the bending of dual-phase steel [35]. These models better describe the Bauschinger effect when material flows through the die radius (bending and strengthening), but additional special cyclic loading of samples needs to be done [36]. Thus, the next work will use such a model to simulate the deep drawing of the cups presented.

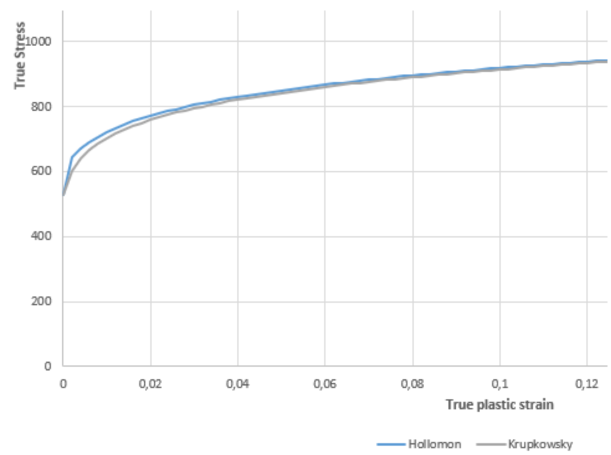

Fig. 13 Comparison of strain-hardening laws

CONCLUSION

3D scanning is increasingly being utilised in stamping plants to assess the quality of pressings due to its automation and rapid data processing capabilities, aligning with the principles of Industry 4.0. This research compares the surfaces of pressings made from dual-phase steel with those predicted by numerical simulations of the deep drawing process for cups with hemispherical and flat bottoms. Two techniques were employed to capture the actual surface: the photogrammetric system Argus and 3D scanning using GOM Scan 1. In the simulations, two constitutive equations describing material behavior were applied. Based on the evaluation of the data, the following outcomes can be drawn:

- Surface comparisons using photogrammetry (nominal surface) and optical scanning showed good correlation, demonstrating that 3D scanning is a valid method for evaluating pressing shapes. The deviations in surface measurements were within +0.04 mm to -0.07 mm for the volume MV 400 used during scanning.
- The comparison between the scanned surface and the numerical simulation results revealed similar outcomes for both constitutive laws applied. The equations of Hill48 and Hollomon used in the numerical simulation demonstrated lower deviations for both flat and hemispherical-bottomed cups, even though these cups exhibit different stress-strain conditions during the process.

Future research will focus on applying hardening rules that consider the Bauschinger effect and exploring more complex pressing shapes beyond cylindrical cups.

Acknowledgement:
This work was supported by the Scientific Grant Agency of the Slovak Republic within the project VEGA 1/0238/23 "Implementation of CAx systems and virtual engineering techniques in the redesign of car-body parts for deformation zones" and VEGA 1/0609/25 "Research and development of methodologies for the assessment of strains of sheet metal and manufacturability of the car components in a virtual environment".

REFERENCES

1. A. Hrivňák, E. Evin: *Formability of steel sheets*. 1st ed., Košice-Elfa, 2004.
2. T. Trzepieciński: Acta Metallurgica Slovaca, 26(2), 2020, 42-44. https://doi.org/10.36547/ams.26.2.553
3. A. Pilar Valerga Puerta, R. Aletheia Jimenez-Rodriguez, S. Fernandez-Vidal, S. Raul Fernandez-Vidal: Photogrammetry as an Engineering Design Tool, In: *Product Design*, Eds.: C. Alexandru, C. Jaliu, M. Comsit, Rijeka: IntechOpen, 2020. https://doi.org/10.5772/intechopen.92998
4. M. Javaid, A. Haleem, R.P. Singh, R. Suman: Sensors International, 2, 2021, 100114. https://doi.org/10.1016/j.sintl.2021.100114
5. M. Bilušić, L. Olivari: Journal of Industrial Information Integration, 41, 2024, 100654. https://doi.org/10.1016/j.jii.2024.100654
6. T. Schenk: *Introduction to Photogrammetry*, Department of Civil and Environmental Engineering and Geodetic Science, The Ohio State University: Columbus, OH USA, 2005.
7. J. Valença, E.N.B.S. Júlio, H.J. Araújo: Experimental Techniques, 36(5), 2012, 71-81. https://doi.org/10.1111/j.1747-1567.2011.00731.x
8. H. G. Maas, U. Hampel: Photogrammetric Engineering & Remote Sensing, 1, 2006, 39-45, https://doi.org/10.14358/PERS.72.1.39
9. J. Baqersad, P. Poozesh, Ch. Niezrecki, P. Avitable: Mechanical Systems and Signal Processing, 86(B), 2017, 17-34. https://doi.org/10.1016/j.ymssp.2016.02.011
10. J. Vagovský, I. Buranský, A. Görög: Procedia Engineering, 100, 2015, 1198-1206. https://doi.org/10.1016/j.proeng.2015.01.484
11. R. Mendricky: MM Science Journal, 10, 2015, 711-716. https://doi.org/10.17973/MMSJ.2015_10_201541
12. Z. Xi, J. Zhou, B. Yang, Y. Zhang, Z. Zhang, D. Li: Measurement, 229, 2024, 114482. https://doi.org/10.1016/j.measurement.2024.114482
13. F. Pourboghrat, E. Chu: International Journal of Mechanical Sciences, 37(3), 1995, 327-341. https://doi.org/10.1016/0020-7403(95)93523-9.F.
14. S. Li, X. Feng: Mechanical Systems and Signal Processing, 135, 2020, 106405. https://doi.org/10.1016/j.ymssp.2019.106405
15. M. Firat, B. Kaftanoglu, O. Eser: Journal of Materials Processing Technology, 196(1–3), 2008, 135-148. https://doi.org/10.1016/j.jmatprotec.2007.05.029
16. M.G. Lee, D. Kim, Ch. Kim, M. L. Wenner, K. Chung: International Journal of Plasticity, 21(5), 2005, 915-953. https://doi.org/10.1016/j.ijplas.2004.05.014
17. W.D. Carden, L.M. Geng, D.K. Matlock, R.H. Wagoner: International Journal of Mechanical Sciences, 44(1), 2002, 79-101. https://doi.org/10.1016/S0020-7403(01)00082-0
18. W. Frącz, F. Stachowicz, T. Pieja: Acta Metallurgica Slovaca, 19(1), 2013, 51-59. https://doi.org/10.12776/ams.v19i1.86
19. H. Yang, H. Li, J. Ma, Z. Zhang, J. Chen: International Journal of Mechanical Sciences, 157–158, 2019, 574-598. https://doi.org/10.1016/j.ijmecsci.2019.05.004
20. W.L. Oberkampf, S.M. DeLand, B.M. Rutherford, K.V. Diegert, K.F. Alvin: Reliability Engineering & System Safety, 75(3), 2002, 333-357. https://doi.org/10.1016/S0951-8320(01)00120-X
21. P. Mulidrán, E. Spišák, M. Tomáš, J. Majerníková, J. Varga: Acta Metallurgica Slovaca, 30(1), 2024, 41-46. https://doi.org/10.36547/ams.30.1.2003
22. ISO 6892-1:2019; Metallic Materials—Tensile Testing—Part 1: Method of Test at Room Temperature. International Organization for Standardization: Geneva, Switzerland, 2019.
23. ISO 10113:2020; Metallic Materials—Sheet and Strip—Determination of Plastic Strain Ratio. International Organization for Standardization: Geneva, Switzerland, 2020.
24. ISO 10275:2020; Metallic Materials—Sheet and Strip—Determination of Tensile Strain Hardening Exponent. International Organization for Standardization: Geneva, Switzerland, 2020.
25. ISO 10360-10:2021; Geometrical product specifications (GPS) — Acceptance and reverification tests for coordinate measuring systems (CMS) — Part 10: Laser trackers. International Organization for Standardization: Geneva, Switzerland, 2021.
26. T. Trzepieciński: Metals, 9, 2019, 988. https://doi.org/10.3390/met9090988
27. R. Hill: Proceedings of the Royal Society, 193, 1948, 281–297. https://doi.org/10.1098/rspa.1948.0045
28. Z. Gronostajski: Journal of Materials Processing Technology, 106(1-3), 2000, 40-44. https://doi.org/10.1016/S0924-0136(00)00635-X
29. H. Vegter, C. ten Horn, M. Abspoel: International Journal of Material Forming, 4, 2011, 85-92. https://doi.org/10.1007/s12289-010-1006-7
30. D. M. Neto, M. C. Oliveira, J. L. Alves, L. F. Menezes: Materials & Design, 60, 2014, 368-379. https://doi.org/10.1016/j.matdes.2014.04.008
31. R. Čada, T. Pektor: Development of a low-cost drawing tool for a press brake, *Metal 2021*, Brno: Tanger, 2021, pp. 241-246. https://doi.org/10.37904/metal.2021.4117
32. M. Abspoel, M. E. Scholting, M. Lansbergen, Y. An, H. Vegter: Journal of Materials Processing Technology, 248, 2017, 161-177. https://doi.org/10.1016/j.jmatprotec.2017.05.006
33. R. Pereira, N. Peixinho, S. L. Costa: Metals, 14(4), 2024, 394. https://doi.org/10.3390/met14040394
34. Mat-Wizard by ESI Group. ESI Group: Paris, France, 2020. [29.8.2024], https://myesi.esi-group.com/addons/esi-mat-wizard
35. P. Mulidran, E. Spišák, M. Tomáš, J. Majerníková, J. Bidulská, R. Bidulský: Materials, 16(2), 2023, 811. https://doi.org/10.3390/ma16020811
36. D. Korečok, P. Solfronk, J. Sobotka: Manufacturing Technology, 20(5), 2020, 625-631. https://doi.org/10.21062/mft.2020.103